ACS NANO

www.acsnano.org

ARTICLE

High-Density and Well-Aligned Hierarchical Structures of Colloids Assembled under Orthogonal Magnetic and Electric Fields

Md Ashraful Haque,[▽] Joseph R. Maestas,[▽] Xingrui Zhu, Benjamin L. Hanson, David T. Wu,* and Ning Wu*

Cite This: https://doi.org/10.1021/acsnano.4c11957

Read Online

ACCESS | Metrics & More | Article Recommendations | Supporting Information

ABSTRACT: Colloids can be used either as model systems for directed assembly or as the necessary building blocks for making functional materials. Previous work primarily focused on assembling colloids under a single external field, where controlling particle−particle interactions is limited. This work presents results under a combination of electric and magnetic fields. When these two fields are orthogonally applied, we can independently tune the magnitude and direction of the dipolar attraction and repulsion between the particles. As a result, we obtain well-aligned, highly dense, but individually separated linear chains at intermediate particle concentrations. Both the inter- and intrachain spacings can be tuned by adjusting the particle concentration and relative strengths of both fields. At high particle concentrations and by tuning the electric field frequency, the individual microspheres can assemble into colloidal oligomers such as trimers, tetramers, heptamers, and nonamers in response to the electric field due to the synergy between dipolar and electrohydrodynamic interactions. These oligomers, in turn, serve as building blocks for making hierarchical structures with finer architectures upon superimposing a one-dimensional (1D) magnetic field. In addition to experiments, Monte Carlo (MC) simulations have been performed on colloids confined near the electrode, interacting through a Stockmayer-like potential. They faithfully reproduce key observations in the experiments. Our work demonstrates the potential of using orthogonal electric and magnetic fields to assemble diversified types of highly aligned structures for applications in high-strength composites, optical materials, or structured battery electrodes.

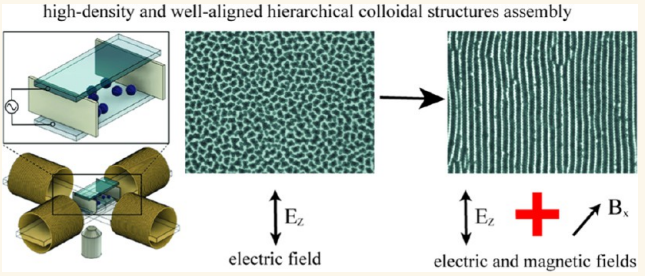

KEYWORDS: *directed assembly, electric field, magnetic field, hierarchical structures, dipolar interaction*

Colloids have been used as model systems for investigating fundamental phenomena in materials science, such as crystallization, phase transition, and glass formation. Additionally, the arrangements of colloids in one, two, or three dimensions can remarkably enhance the mechanical, optical, or electrical properties of functional materials.[1−9] Therefore, acquiring the ability to direct the assembly of colloids with fine architectures has remained a compelling driving force behind extensive research efforts over the past decade.[10−16]

Among the myriad approaches to colloidal assembly, the use of externally applied electric and magnetic fields has garnered significant interest. These fields induce dipolar interactions among colloids, swiftly leading to diverse structures, including microlassos,[14] colloidal switches,[17] chiral clusters,[18] and colloidal molecules.[19−21] Furthermore, the magnitude and effective range of these dipolar interactions can be tuned conveniently by varying the field's strength or frequency.[16] Notably, one-dimensional (1D) magnetic or electric fields have been widely used to align fillers such as nanospheres, nanotubes, and platelets into linear chains within composite materials. This alignment enhances mechanical strength[26−28] or improves the ionic conductivity of battery electrodes.[29,30] They have also been used to tune the structure and rheological properties of fluids.[31,32]

However, those chain-like structures often lack precise control, particularly at high particle concentrations, where strong and short-range dipolar attractions between chains often

Received: August 28, 2024
Revised: December 18, 2024
Accepted: December 23, 2024

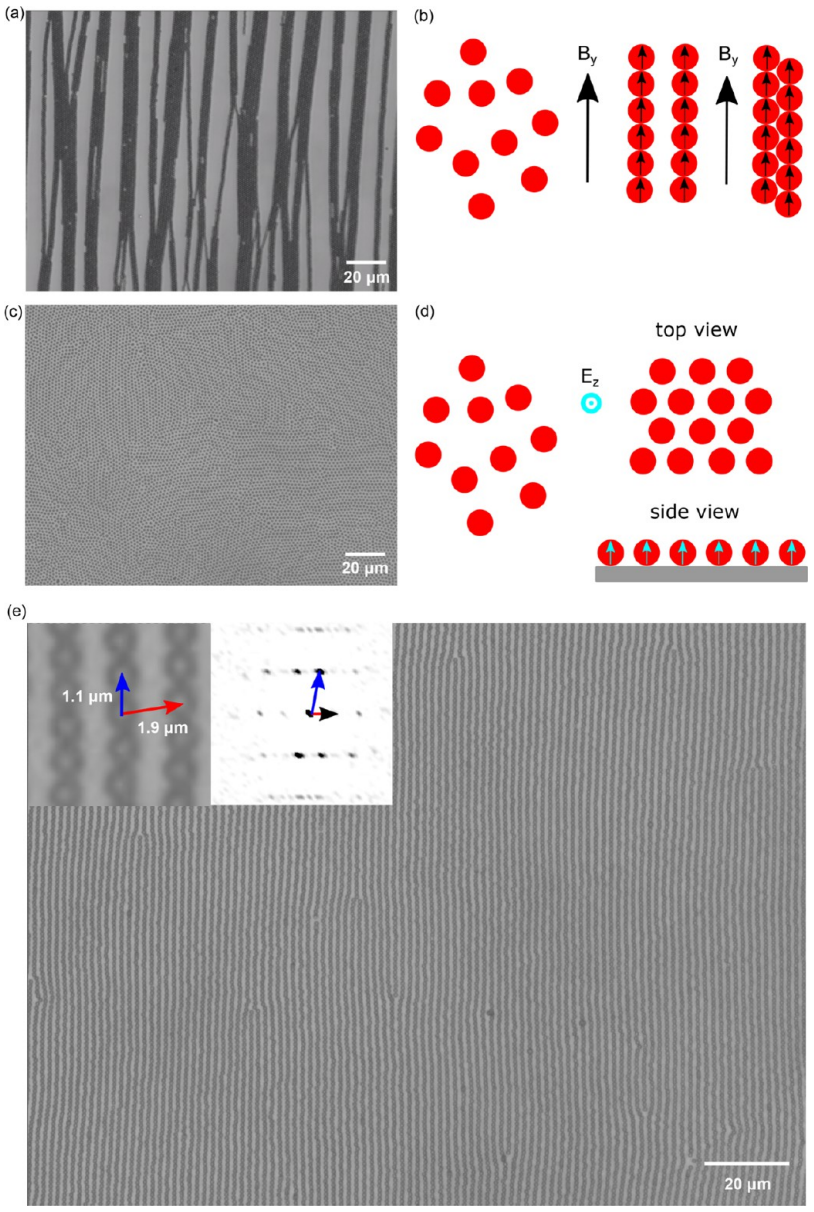

Figure 1. Colloidal monolayers are assembled under magnetic and electric fields. (a) Optical image of bundles of linear chains formed by a one-dimensional AC magnetic field parallel to the *y*-axis. B_y = 4.25 mT, f_B = 50 Hz, and η_L = 0.510. (b) Schematic showing the assembly of microspheres into linear chains and bundles. Black arrows represent the magnetic field and induced magnetic dipoles. (c) Optical image of the nonclose-packed hexagonal array formed under an AC electric field parallel to the *z*-axis (E_z = 10^5 V/m, f_E = 1,300 Hz, and η_L = 0.510). (d) Schematic showing the assembly of microspheres into hexagonal arrays. Cyane arrows represent the induced electric dipoles. (e) Optical image of high-density and well-aligned colloidal chains when the magnetic and electric fields are superimposed (E_z = 10^5 V/m, f_E = 1,300 Hz, B_y = 4.25 mT, f_B = 50 Hz, and η_L = 0.374). The insets show a magnified area of the chains and the diffraction pattern of the whole image.

result in the formation of aggregated bundles and fibrous structures with nonuniform spacing. This limitation arises because, under the influence of a single external field (electric or magnetic), the nature of dipolar interactions (i.e., attraction vs repulsion) cannot be independently controlled. Instead, it depends on the angle between the separation vector of the particles' centers and the direction of the applied field. Such a deficiency motivates this work that combines orthogonally applied electric and magnetic fields to fabricate high-density and well-aligned hierarchical structures of colloids.

When magnetic and electric fields are compared, it may initially appear that the structures formed under one type of field could also be achieved by the other because a magnetic dipole is mathematically equivalent to an electric dipole. However, as we will elucidate in this paper, subtle yet significant distinctions exist between these two fields, both conceptually and practically.[33] To begin, a noteworthy distinction is the absence of free magnetic monopoles. In contrast, ions in a solvent can readily respond to the applied electric field, resulting in intricate electrohydrodynamic flow patterns around the particles depending on the frequencies.[34−36] More often than not, these electrohydrodynamic effects introduce additional mechanisms through solvent-mediated interactions, enabling the formation of complex structures that cannot be attainable by magnetic fields alone. Furthermore, the presence of a conducting substrate (i.e., the electrode) introduces another layer of complexity. The substrate serves as an equipotential surface and, as such,

https://doi.org/10.1021/acsnano.4c11957
ACS Nano XXXX, XXX, XXX−XXX

interacts with particles through forces such as charge-image charge and dipole-image dipole interactions, which influence particle behaviors.

While it is true that electric fields can induce more complex colloidal interactions than magnetic fields, the practical implementation of three-dimensional (3D) electric fields poses significant experimental challenges. This is primarily because different sets of electrodes are needed to generate multiaxial electric fields. Unfortunately, the field generated by one set typically interferes with other fields, leading to a fringing effect and field inhomogeneity within the sample. Moreover, when the samples are not in direct contact with the electrodes, a significant potential drop can occur across the dielectric medium between them, thereby reducing the effective electric field within the sample. In comparison, the generation of multiaxial magnetic fields by assembling several Helmholtz coils in different directions is much easier. No field attenuation or "charge" screened interaction will occur within the sample. Therefore, the combination of electric and magnetic fields, capitalizing on the strength of both, offers a novel avenue to exert precise control over interparticle interactions and, by extension, the assembled structures.[13,37,38]

In this work, we combine a 1D alternating-current (AC) magnetic field parallel to the substrate with a 1D AC electric field oriented perpendicular to the substrate. This combination enables us to effectively direct the assembly of colloidal particles effectively. By inducing two mutually orthogonal electric and magnetic dipoles on each particle, we gain precise control over several aspects independently, including the strength, direction, and nature of the dipolar interactions (i.e., whether they are attractive or repulsive). This level of control allows us to create highly dense and precisely aligned colloidal structures with complex architectures. Our results underscore the tremendous potential of combining these two fields in an orthogonal manner to achieve advanced colloidal assembly.

RESULTS AND DISCUSSION

Our experimental setup is shown in Figure S1. An aqueous solution containing carboxyl functionalized magnetic microspheres (1.05 μm DynaBeads) is sandwiched between two indium−tin oxide (ITO) glass slides separated by h = 100 μm. An AC electric field normal to the substrate (along the z-direction) can be generated between the two ITO slides. In the meantime, four air-cored copper solenoid coils arranged orthogonally in the x-y plane allow us to create two-dimensional (2D) magnetic fields. Under the 1D magnetic field, although particles can be aligned into individual linear chains at low particle concentrations, the assembled chains tend to further aggregate into bundles at intermediate and high particle concentrations (Figure 1a) in response to the uniaxial magnetic field $\mathbf{B} = B_y \cos(2\pi f_B t)\hat{\mathbf{y}}$ (where f_B is the magnetic field frequency and B_y is the field strength). This phenomenon can be understood by considering two adjacent chains in Figure 1b. While there is strong magnetic dipolar repulsion between two chains separated side by side, the total energy can be minimized by staggering them, especially when they are close enough. As such, there is a driving force for the aggregation of neighboring chains until the bundles are separated far enough that the dipolar interaction between them is weak. This process depends sensitively on the local concentration of chains, and as a result, there is often a wide distribution in interbundle spacing.

On the other hand, when a 1D AC electric field $\mathbf{E} = E_z \cos(2\pi f_E t)\hat{\mathbf{z}}$ (where f_E is the electric field frequency and E_z is the field strength) is applied along the z-axis, the same microspheres assemble into a nonclose-packed hexagonal crystal due to the electric dipolar repulsion arising from the induced electric dipoles perpendicular to the substrate (Figure 1c,d). Here, we define the area fraction of the particles as $\eta_L = N_L \pi\sigma^2/4A$, where N_L is the number of bottom-layer particles, σ is the particle diameter, and A is the field of view area. Interestingly, when the two fields are applied orthogonally, we obtain highly dense but well-aligned chains (Figure 1e and Movie S1). While the particles still align into chains due to the in-plane magnetic dipolar attraction, the out-of-plane electric dipolar repulsions cause the chains to remain separated. From the diffraction pattern (inset, Figure 1e), we can determine the separation between the nearest neighboring particles along a chain and the separation between chains. This type of structure can be assembled because the amplitude and direction of the two fields can be tuned independently. As such, the combined magnetic and electric fields generate two orthogonally aligned dipoles, allowing for fine control of the attractive and repulsive interactions. Since the magnetic field is along the y-direction, the induced magnetic dipole on each particle points toward the same direction. The head-to-tail attraction between magnetic dipoles is the driving force for chain formation. However, a side effect is that neighboring chains also feel a driving force to reduce the total energy by staggering together. We resolve this issue by inducing an electric dipole on each particle orthogonal to the magnetic dipoles. As a result, all particles feel a uniform shoulder-to-shoulder electric dipolar repulsion among themselves. This force is weak enough not to interfere with the magnetic alignment of the individual stripes. Still, it is strong enough to prevent the aggregation of neighboring stripes, leading to the pattern shown in Figure 1e.

The same structure cannot be obtained by applying a magnetic field simultaneously along both the y- and z-directions. As shown in Figure S2, individual chains are tilted relative to the substrate. This is because even a weak magnetic field along the z-direction would favor particle chaining along the vertical direction as long as the gravitational energy barrier (small for micro−or nanoparticles) can be overcome. Stronger magnetic fields in the y and z-directions will lead to tilted chains along the overall field direction, and chain bundling is unavoidable if the chains are close to each other. Compared with the magnetic field, there is an additional attraction between the particles and the conducting substrate under the electric field, i.e., the dipole-image dipole attraction, which can attract all particles toward the substrate, making it much harder to form vertical chains. Moreover, we will demonstrate later that electrohydrodynamic flow (and interactions) can be generated under low-frequency electric fields, which creates more complex and intriguing structures that are not possible under magnetic fields alone. Therefore, our work demonstrates the advantages of combining the two fields.

We also used MC simulations to investigate the impacts of relative magnetic and electric field strengths on a monolayer of microspheres. The interaction between particles i and j is modeled by a Stockmayer-like potential

$$U(r_{ij}, \theta_E, \theta_B) = U_{LJ}(r_{ij}) + U_E(r_{ij}, \theta_E) + U_B(r_{ij}, \theta_B) \quad (1)$$

which includes the Lennard-Jones (LJ), electric dipolar, and magnetic dipolar interactions

https://doi.org/10.1021/acsnano.4c11957
ACS Nano XXXX, XXX, XXX−XXX

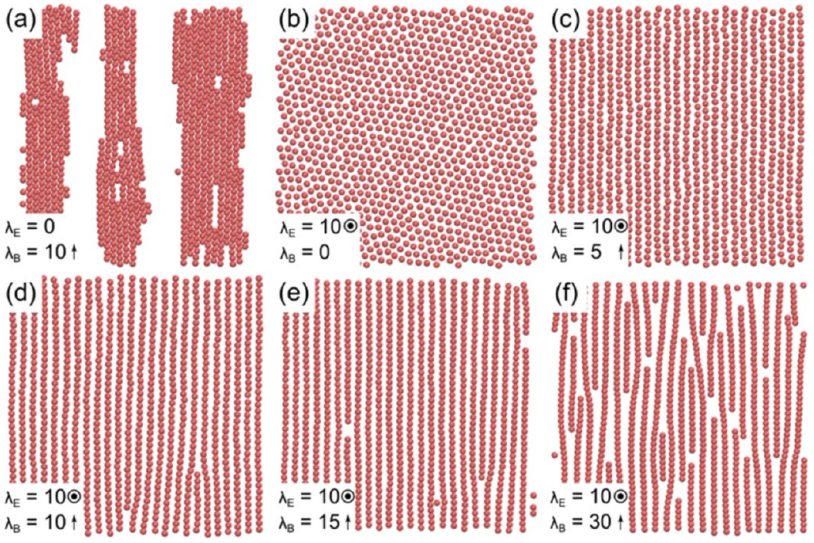

Figure 2. MC simulations reveal the effect of combined electric and magnetic fields. (a) Colloids align into chain bundles in response to a magnetic field only due to in-plane magnetic dipolar attraction. (b) Out-of-plane electric dipolar repulsion causes the particles to assemble into a hexagonal lattice in response to an electric field only. (c–f) When both electric and magnetic fields are applied, particles align into dense but well-separated chains. Insets indicate the strengths and directions of the electric (λ_E) and magnetic (λ_B) interactions. $\eta_L = 0.50$, and $N = 1000$ for all simulations.

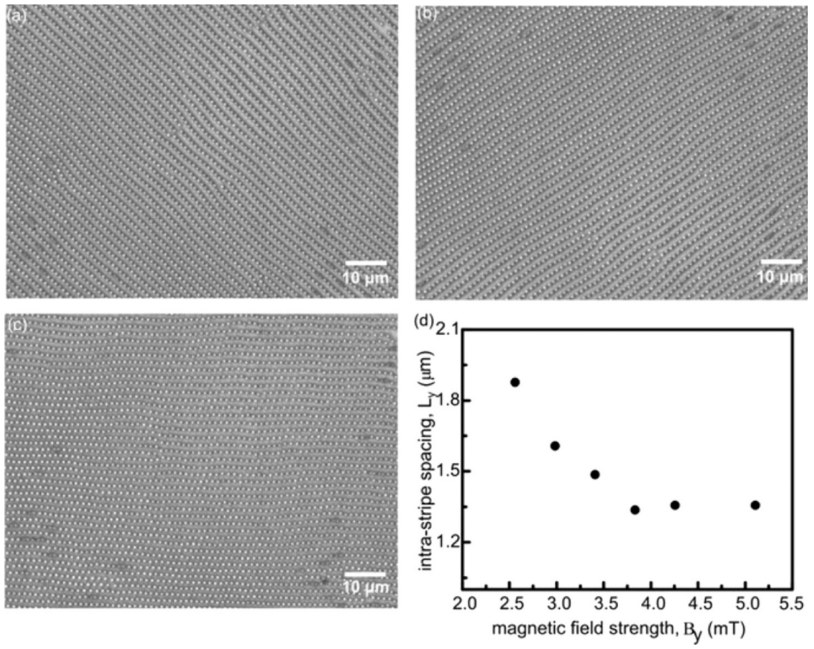

Figure 3. Impact of magnetic field on stripe patterns. The optical images illustrate the chain orientation at different magnetic field conditions. (a) $B_x = 4.25$ mT, $B_y = 4.25$ mT, $\phi = 0°$, and $\eta_L = 0.400$. (b) $B_x = 4.25$ mT, $B_y = 4.25$ mT, $\phi = 180°$, and $\eta_L = 0.400$. (c) $B_x = 4.25$ mT, $B_y = 0$ mT, and $\eta_L = 0.400$. (d) Intrastripe spacing, L_y, can be tuned by the magnetic field strength. The electric field is held constant at $E_z = 10^5$ V/m and at $f_E = 1{,}300$ Hz.

$$U_{LJ}(r_{ij}) = 4\varepsilon_{LJ}\left[\left(\frac{\sigma}{r_{ij}}\right)^{12} - \left(\frac{\sigma}{r_{ij}}\right)^{6}\right] \quad (2)$$

$$U_E(r_{ij}, \theta_E) = \varepsilon_E\left(\frac{\sigma}{r_{ij}}\right)^{3}[1 - 3\cos^2\theta_E] \quad (3)$$

$$U_B(r_{ij}, \theta_B) = \varepsilon_B\left(\frac{\sigma}{r_{ij}}\right)^{3}[1 - 3\cos^2\theta_B] \quad (4)$$

where r_{ij} is the separation between particles i and j, ε_{LJ} is the LJ potential well depth, and σ is the LJ distance parameter. The induced electric (magnetic) dipole moment of a particle is taken to be aligned with the externally applied field direction (electric field along the z-axis and magnetic field along the y-axis). θ_E (θ_B) is the angle formed by vector $\mathbf{r}_{ij}$ and the z-axis (y-

https://doi.org/10.1021/acsnano.4c11957
ACS Nano XXXX, XXX, XXX−XXX

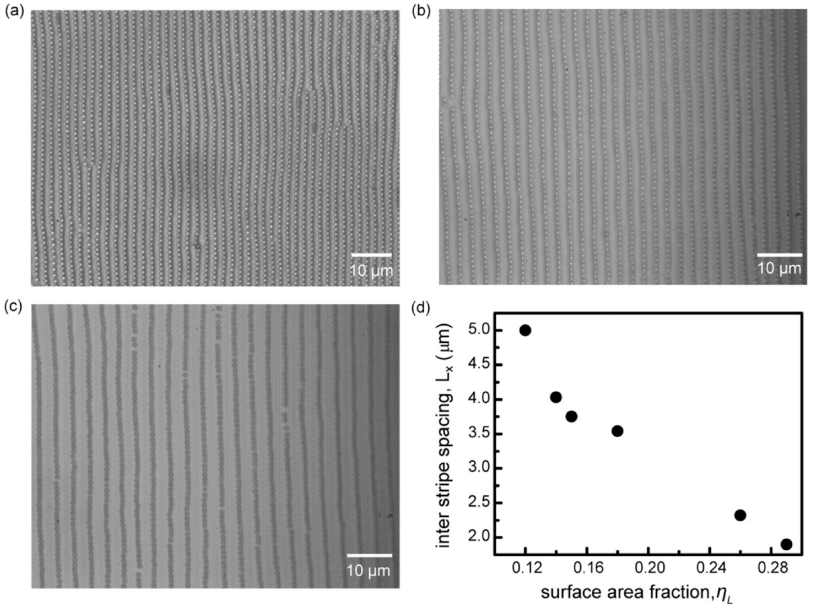

Figure 4. Control of the interstripe spacing by tuning the particle surface area fraction, η. Optical images of the stripe pattern at (a) η_L = 0.248, (b) η_L = 0.186, and (c) η_L = 0.107. (d) Dependence of the interstripe spacing L_x on η_L. B_y = 4.25 mT, f_B = 50 Hz, E_z = 10^5 V/m, and f_E = 1,300 Hz.

axis), as illustrated in Figure S3. The parameter ε_E represents the strength of the electric dipolar interaction energy

$$\varepsilon_E = \pi\epsilon_s\sigma^3 K_E{}^2 E_{rms}{}^2/16 \quad (5)$$

where ϵ_s is the permittivity of the solvent, K_E is the electric Clausius−Mossotti factor, and E_{rms} is the root mean square of the applied electric field. The parameter ε_B characterizes the strength of the magnetic dipolar interaction energy

$$\varepsilon_B = \pi\sigma^3 K_B{}^2 B_{rms}^2/16\mu_s \quad (6)$$

where $K_B = (\mu_p - \mu_s)/(\mu_p + 2\mu_s)$ is the magnetic Clausius−Mossotti factor, $\mu_p(\mu_m)$ is the permeability of the particle (solvent), and B_{rms} is the root mean square of applied magnetic field strength. Here, we choose $\mu_p = 2 \times 10^{-6}$ H/m based on the literature.[22] We define nondimensional parameters $\lambda_E = \varepsilon_E/\varepsilon_{LJ}$ (which characterizes the strength of the electric dipolar interaction) and $\lambda_B = \varepsilon_B/\varepsilon_{LJ}$ (which characterizes the strength of the magnetic dipolar interaction). The relative strength is defined as $\Lambda = \varepsilon_B/\varepsilon_E = \lambda_B/\lambda_E$. Since we fix the z-positions of particles and make them into a monolayer, no particle−electrode interaction needs to be considered in our simulations.

When only a magnetic field (λ_B = 10) is applied along the y-axis, particles align into linear chains along the field direction first. They then aggregate into a staggered configuration, forming dense bundles (Figure 2a), consistent with what was observed in Figure 1a. When only an electric field (λ_E = 10) is applied along the z-axis, repulsive interactions between particles induce a nonclose-packed hexagonal array (Figure 2b). With the combined fields (Λ = 0.5), the hexagonal array reorganizes and assembles into loosely aligned chains (Figure 2c). This critical ratio of Λ can be understood by considering the magnitude of the electric and magnetic dipolar interactions between a pair of spheres at contact. The electric dipolar repulsion $U_E = \varepsilon_E$ because $\theta_E = 90°$, while the magnetic dipolar attraction $U_B = -2\varepsilon_B$ since $\theta_B = 0°$. Therefore, a linear chain can only be formed when $|U_B| \geq |U_E|$, or equivalently $\Lambda = \varepsilon_B/\varepsilon_E = \lambda_B/\lambda_E \geq 0.5$. With increasing magnetic field strength, the chains become more aligned, and particles within each chain are more close-packed (Figure 2d,e). Interestingly, at high magnetic field strength (e.g., Λ = 3), the long chains break into shorter ones. In a chain segment exposed to high magnetic field strengths, the two end particles experience a strong pull from neighboring particles, placing the segment under tension that could cause it to break into shorter chains. This might explain the observation of shorter chains in simulations under very strong magnetic fields. However, simulations with longer time scales and larger simulation boxes would be required to fully understand this phenomenon.

We further investigated how both fields can control the chain patterns. First, we show that the applied magnetic field, $\mathbf{B} = B_x\cos(2\pi f_B t)\hat{\mathbf{x}} + B_y\cos(2\pi f_B t + \phi)\hat{\mathbf{y}}$, can control the chain orientations. Here, B_x (B_y) is the magnitude of the x- (y-) component of the magnetic field strength, and ϕ is the phase angle. As shown in Figure 3a,b, when $B_x = B_y$ and $\varphi = 0°$ (or 180°), the chains are oriented 45° (or −45°) relative to the x-axis. Horizontally oriented chains can be obtained when $B_y = 0$ (Figure 3c). The chain orientation can be conveniently adjusted by tuning either the field strength or the phase angle between the magnetic fields along the x- and y-axes. As the magnetic field direction changes, long chains break into shorter ones (~3−4 colloids long) before quickly reassembling and aligning with the field (Movie S2). Furthermore, the intrachain spacing (L_y), i.e., the separation between neighboring particles along the same chain, can be tuned by the magnetic field strength (Figure 3d). As the magnetic dipolar interaction is proportional to the square of the field strength, stronger magnetic fields can drastically reduce the intrachain spacing until the electrostatic repulsion between neighboring particles balances the magnetic attraction.

The interstripe separations (L_x) can also be tuned by changing the particle area fraction. As shown in Figure 4, with increasing particle area fraction, the interstripe spacing decreases under the same magnetic and electric field conditions. Figure 4d shows that L_x is approximately inversely

https://doi.org/10.1021/acsnano.4c11957
ACS Nano XXXX, XXX, XXX−XXX

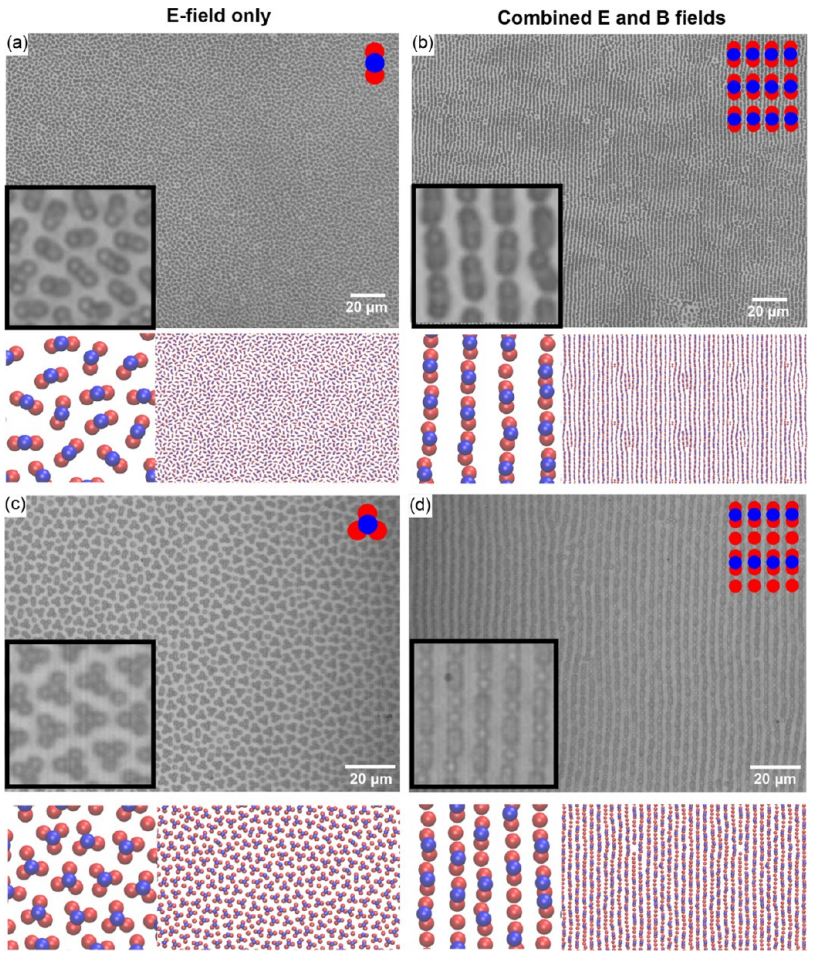

Figure 5. Chains were assembled from colloidal trimers and tetramers. In each image, experiment results are shown on the top. The ideal structure is shown schematically in the upper right corner, while the left insets zoom in on the structure. The simulation results are shown at the bottom. Red (blue) spheres represent particles in the lower (upper) layer. (a) Trimers formed in response to an electric field only (experiment: E_z = 10^5 V/m, f_E = 2,000 Hz, and η_L = 0.241; simulation: λ_E = 10, γ = 1:2, and η_L = 0.270). (b) Aligned chains assembled from the trimers in part (a) upon superposition of a 1D orthogonal magnetic field (experiment: B_y = 5.1 mT and η_L = 0.257; simulation: λ_B = 5 and η_L = 0.270). (c) Tetramers formed in response to an electric field only (experiment: E_z = 10^5 V/m, f_E = 750 Hz, and η_L = 0.385; simulation: λ_E = 10, γ = 1:3, and η_L = 0.367). (d) Aligned chains assembled from the tetramers in part (c) upon superposition of a 1D orthogonal magnetic field (experiment: B_y = 5.1 mT and η_L = 0.376; simulation: λ_B = 5 and η_L = 0.367).

proportional to η_L, i.e., $L_x \propto {\eta_L}^{-1}$. By definition, $\eta_L = N_L\pi\sigma^2/A$. For a given field of view area A, the number of particles N_L is inversely proportional to the intrachain spacing L_x. Therefore, it is expected that the interchain spacing is inversely proportional to the area fraction. However, the spacing cannot be reduced below ~1.5 μm; as the particle concentration increases further, the microspheres can no longer maintain a monolayer array.

Individual particles can assemble into small nonplanar colloidal clusters at high particle concentrations and under a low-frequency AC electric field alone.[19,20] For example, at f_E = 2,000 Hz, linear trimers in which a central sphere sits on the top of two bottom spheres are observed (Figure 5a). Pyramid-like tetramers in which a sphere in the upper layer is associated with three spheres in the lower layer can be found at a lower frequency, e.g., f_E = 750 Hz, as shown in Figure 5c. The formation of those 3D oligomers can be attributed to the synergy between the out-of-plane head-to-tail electric dipolar attraction and electrohydrodynamic (EHD) flow, as discussed in our previous work.[19,23] At high particle concentrations, the in-plane electric dipolar repulsion prevents more particles from forming a monolayer. Instead, some particles tend to jump on top of others, and the out-of-plane electric dipolar attraction facilitates the association of the central top particles with the bottom petal particles (blue and red particles in Figure 5a). Although there is an energy barrier in switching from dipolar repulsion to attraction (as the angle, θ_E, between the interparticle separation vector ($\mathbf{r}_{ij}$) and the electric field ($\mathbf{E}$) needs to be less than the magic angle of ~54.7°),[39] this energy barrier can be significantly reduced by an additional extensile EHD flow near each particle at low frequencies. As illustrated in Figure S4, this extensile and circulating flow[40] repels neighboring particles on the substrate but attracts them (in bulk) back toward the void between the bottom-layer particles. It facilitates the formation of nonplanar clusters but prevents vertical chain formation along the direction of the electric field, although it is more energetically favorable from the dipolar interactions alone. Indeed, since EHD flow is inversely proportional to frequency,[41] the nonplanar clusters disassemble and vertical chains are observed at frequencies above 20 kHz, where EHD flow diminishes and dipolar interactions dominate.

https://doi.org/10.1021/acsnano.4c11957
ACS Nano XXXX, XXX, XXX−XXX

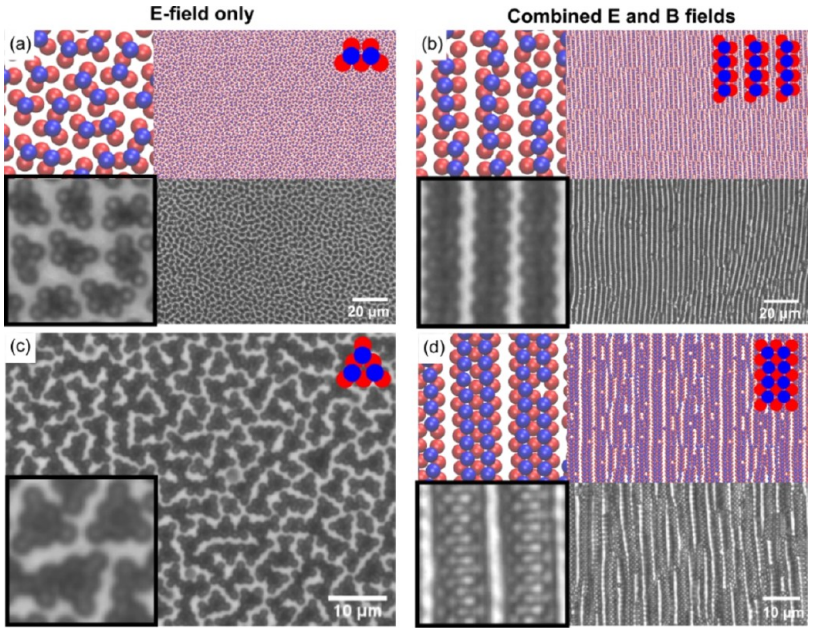

Figure 6. Well-aligned chains formed by colloidal heptamers and nonamers. (a) Butterfly-like heptamers formed in response to an electric field only (experiment: $E_z = 10^5$ V/m, $f_E = 450$ Hz, and $\eta_L = 0.486$; simulation: $\lambda_E = 11$, $\gamma = 2{:}5$, and $\eta_L = 0.459$). (b) Aligned zipper-like stripes formed by the heptamers in part (a) upon superposition of a 1D orthogonal magnetic field (experiment: $B_y = 5.1$ mT and $\eta_L = 0.475$; simulation: $\lambda_B = 4$ and $\eta_L = 0.459$). (c) Triangular nonamers formed in response to an electric field only (experiment: $E_z = 5 \times 10^4$ V/m, $f_E = 350$ Hz, and $\eta_L = 0.752$). (d) Aligned double-column bundles formed by the nonamers in part (c) upon superposition of a 1D orthogonal magnetic field (experiment: $B_y = 5.1$ mT and $\eta_L = 0.771$; simulation: $\lambda_E = 7$, $\lambda_B = 5$, $\gamma = 2{:}3$, and $\eta_L = 0.790$). While the nonamers in part (c) cannot be simulated, the structures in part (d) were obtained in the simulation by choosing an initially random distribution of particle bilayers with $\gamma = 2{:}3$.

In our previous work,[23] we have successfully modeled the formation of clusters in MC simulations by confining the particles to bilayers and tuning the ratio of the numbers of the upper-plane to lower-plane particles, i.e., $\gamma = N_U/N_L$. For example, by choosing $\gamma = 1{:}2$ and using the corresponding experimental field strength and particle concentration, we simulated the assembly of spheres into trimers, while tetramers (Figure 5c) can be obtained by setting $\gamma = 1{:}3$. As such, we demonstrate that the correct γ is needed to assemble clusters of different sizes, which can be achieved in experiments by tuning the particle concentration, field strength, and frequency. Note that EHD flow and hydrodynamic interactions are not explicitly considered in our MC simulations because the hydrodynamic interactions are not additive. However, by confining the particles in bilayers, we can still capture the formation of smaller clusters since they are held together primarily by dipolar interactions. We also emphasize that EHD flow occurs at low particle concentrations, too. In a monolayer of well-separated particles, the extensile EHD flow generates hydrodynamic repulsion between neighboring particles. The far-field approximation of this repulsion scales with $1/r^3$,[41] similar to the electric dipolar repulsion. Consequently, although EHD interactions are not included in our simulations in Figure 2, they can still capture the essential structures and dynamics of chain formation at low particle concentrations.

The assembly of nearly monodisperse colloidal clusters such as trimers and tetramers under an electric field allows us to conveniently investigate the influence of magnetic fields on building blocks beyond simple microspheres. As shown in Figure 5a,b, while the trimers assembled under the electric field alone are randomly oriented, they realign into trimeric stripes when a 1D AC magnetic field is superimposed along the y-axis. Here, both the magnetic (in-plane head-to-tail) and electric (out-of-plane head-to-tail) dipolar interactions favor the alignment of the trimers. In contrast, the tetramers can no longer preserve their shapes in response to the additional magnetic field (Figure 5c,d) due to the strong magnetic alignment along the y-direction. Instead, the tetramers are disassembled into trimers and monomers arranged alternately into stripes. Under the corresponding experimental conditions, the simulated structures in Figure 5b,d closely resemble our experimental results. Therefore, we find a route to introduce finer architectures into the aligned stripes using more complex building blocks than colloidal spheres assembled by the electric field.

Stripes with more exotic structures can be made using other building blocks assembled at lower electric field frequencies and higher particle concentrations. For example, at $f_E = 450$ Hz, two neighboring tetramers can further assemble into a butterfly-like heptamer, in which they share a common lower-plane particle (Figure 6a). In simulations, we found that similar clusters can be modeled by setting $\gamma = 2{:}5$. Similar to what is observed in experiments, we note that the butterfly clusters tend to be stable at higher concentrations. At an even lower frequency, i.e., $f_E = 350$ Hz, triangular nonamers are assembled from three tetramers, each sharing two lower-plane particles with the other tetramers (Figure 6c). The dependence of the cluster size on frequency (i.e., from trimer to nonamer) is consistent with our hypothesis that the extensile EHD flow reduces the energy barrier for switching from dipolar repulsion between particles in the same plane to dipolar attraction between particles located in different planes. As the EHD flow becomes stronger at low frequencies, larger clusters (formed by five or more particles) are observed. While the formation of

https://doi.org/10.1021/acsnano.4c11957
ACS Nano XXXX, XXX, XXX−XXX

large clusters is primarily driven by frequency, higher particle concentrations tend to yield a more uniform distribution of building blocks within the field of view. This strategy creates a favorable pathway for assembling particles into heptamers, nonamers, and larger clusters. We note that our Monte Carlo simulations do not produce nonamer structures, likely due to the omission of complex near-field EHD interactions, which are critical in forming close-packed colloidal clusters and the mutual dipole model at high particle concentrations. Nevertheless, our previous results,[23] along with other results presented in this work, demonstrate that the Stockmayer-like potential is sufficient to model the electric-field-directed assembly of colloids in most cases.

Similar to what is observed with the trimers and tetramers, arrays of heptamers and nonamers reconfigure in response to the addition of a magnetic field (5.1 mT) along the *y*-axis. As shown in Figure 6b, the heptamers reorient and assemble into zipper-like stripes to maximize the gain in magnetic energy. We observe a similar behavior in our simulation when the relative magnetic dipole strength is $\Lambda \sim 0.36$. Unlike the transition of trimers and tetramers into stripes, which occurs at constant γ, we note that the transition from heptamers to zipper-like stripes occurs with a small change in γ (γ = 2:5 vs γ = 1:2). Therefore, some defects exist in the zipper-like stripes due to a lack of upper plane particles initially. Similarly, the nonamers become unstable in response to the magnetic field as particles reorganize into wide columns consisting of rectangular unit cells (Figure 6d). Arguably, they are equilibrium structures that minimize the sum of magnetic and electric energies. While the nonamer structures in Figure 6c are not observed in our simulations, we find that the double-column stripes could still be reproduced in simulations (Figure 6d) by choosing an initially random distribution of particle bilayer with γ = 2:3. We note that the formation of colloidal clusters serves as excellent kinetic intermediates for developing the complex striped patterns in Figures 5 and 6. Experimentally, applying electric and magnetic fields simultaneously at high particle concentrations can also yield hierarchical stripes, although this approach typically results in a higher number of defects.

We have performed more simulations with varying the upper to lower-plane particle ratio (γ), particle concentration (η_L), and relative magnetic field strength (Λ) to better understand the impacts of these parameters on the stripe architectures. In all simulations, particles were randomly distributed initially to mimic our experiments. The electric and magnetic fields were applied simultaneously. The equilibrium structures, however, do not differ from what is obtained when an electric field is applied before the introduction of a magnetic field or vice versa. When γ = 1:1, straight stripes of dimers align along the *y*-axis, formed by pairs of an equal number of red and blue particles (Figure 7a). Particles in each plane are in contact with the nearest neighbor along an individual stripe. Such a structure is primarily stabilized by a strong magnetic field (Λ = 1). When γ is changed to 1:3 and η_L is changed to 0.60, we find a mixture of pentameric stripes and chains of monomers, as shown in Figure 7b. In Figure 7c, when γ = 1:2 but with Λ = 0.7 and η_L = 0.67, we obtain an array of columns where a single upper plane stripe (blue) is surrounded by two stripes of the bottom plane particles (the red). This structure is noticeably different from the array of trimeric stripes shown in Figure 5b. The difference in stripe architecture is caused by increasing the area fraction. At η_L = 0.60, particles in the lower plane prefer to be assembled into square tiles, forming the base of a pentamer unit cell. Finally, with γ = 2:3 but a relatively low field strength ratio (Λ = 0.2), the stronger in-plane repulsive electric dipolar interactions increase the spacing between particles within each stripe. As a result, we observed stripes of rectangular bands (Figure 7d). As the magnetic field increases, the rectangular bands become denser, eventually evolving into double-column bundles in Figure 6d. Therefore, our simulation results show that particle ratio γ, particle area fraction η_L, and relative field strength Λ can all be used to fine-tune the architectures of various hierarchical stripes.

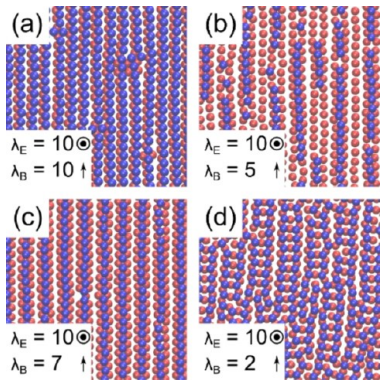

Figure 7. Effects of upper to lower-plane particle ratio (γ), particle density (η_L), and relative field strength (Λ) on chain architecture. (a) Dimeric stripes (γ = 1:1, η_L = 0.57, and Λ = 1.00). (b) Mixture of pentameric stripes and chains of monomers (γ = 1:3, η_L = 0.60, and Λ = 0.50). (c) Pentameric stripes (γ = 1:2, η_L = 0.67, and Λ = 0.70). (d) Stripes of rectangular bands (γ = 2:3, η_L = 0.60, and Λ = 0.2).

The AC electric field used in this study is necessary to prevent water electrolysis and to enable additional control over colloidal cluster formation and EHD flow through frequency adjustments. While a one-dimensional DC field could replace the AC magnetic field with similar effects, tuning the frequency and phase angle of AC magnetic fields along the *x*- and y-axes offers further versatility. This approach could enable the formation of novel colloidal structures in future studies.

CONCLUSIONS

In this work, we present a strategy to control the spatial arrangement of colloidal microspheres, resulting in high-density and well-aligned stripes with finely tuned architectures. This is achieved by simultaneously applying orthogonal electric and magnetic fields. The combined fields generate orthogonally aligned electric and magnetic dipoles on each particle, enabling us to independently manipulate the magnitude and direction of both attractive and repulsive dipolar interactions between the particles. As a result, we obtain high-density arrays of well-aligned and individually separated stripes. Furthermore, exploiting the synergistic effects arising from the interplay between electric dipolar interactions and electrohydrodynamic flow at high particle concentrations and low frequencies, we were able to generate new types of colloidal clusters such as linear trimers, pyramid tetramers, butterfly-like heptamers, and triangular nonamers. Upon the superposition of a 1D magnetic field, these colloidal clusters, as new and more complex building blocks, were assembled into stripes and columns with hierarchical microstructures, depending on the initial configurations of the colloidal cluster arrays. Furthermore, the structures can be reconfigured and relaxed within a short time scale of approximately 1 s by toggling the electric and magnetic

https://doi.org/10.1021/acsnano.4c11957
ACS Nano XXXX, XXX, XXX−XXX

field strengths, highlighting their potential for use in stimuli-responsive materials.

The experimental findings in this study are further complemented by MC simulations, where particles are confined to either a monolayer or a bilayer arrangement and interact through a Stockmayer-like potential. These simulations are conducted using a variety of tunable parameters, including particle concentration, electric and magnetic field strength, and the ratio of particles between the upper and lower planes. Our MC simulations faithfully reproduce many colloidal structures observed in our experiments. Moreover, our simulations unveil additional types of stripe formation, achievable through fine-tuning the upper plane to lower-plane particle ratio and the relative strengths of the electric and magnetic fields. This not only validates our experimental results but also offers valuable insights into the creation of new structures in future endeavors. Collectively, our research underscores the advantages of leveraging orthogonally aligned electric and magnetic fields to steer the colloidal assembly. This approach not only provides a versatile tool for generating a variety of highly aligned structures but also holds promise for applications in making high-strength composites, advanced optical materials, and structured battery electrodes.

EXPERIMENTAL AND COMPUTATIONAL SECTION

Materials. Composite magnetic particles (Dynabeads MyOne Carboxylic Acid, 1.05 μm in diameter) were purchased from Thermo Fisher Scientific (Waltham, MA). Indium−tin oxide (ITO) glass slides (sheet resistance 15−25 Ω/square) were purchased from Sigma-Aldrich. Polyester films (100 μm thick) were purchased from Micron Wings. Solvents such as acetone and 2-propanol (99%) were purchased from Pharmco. Poly(sodium 4-styrenesulfonate) (molecular weight = 70,000) was purchased from Sigma-Aldrich.

Experimental Setup. Our experimental setup is shown in Figure S1. Two ITO glass slides were used as the bottom and top electrodes. The ITO electrodes were treated to prevent particles from adhering to their surfaces. They were first cleaned with acetone and isopropanol for 15 min inside an ultrasonic bath. They were then exposed to oxygen plasma for 1 min, making them hydrophilic. As a final step, the electrodes were coated with aqueous poly(sodium 4-styrenesulfonate) solution (5 mg/mL), giving them a negative surface charge. As a result, the carboxyl functionalized DynaBeads experience electrostatic repulsion from the electrodes. A pair of nonconducting polyester films were used as spacers (h = 100 μm), forming a chamber between the two electrodes. In a typical experiment, 5−10 μL of dilute Dynabeads solution in deionized water was added between the two electrodes. An AC electric field was applied perpendicular to the two ITO electrodes via an AC function generator (RIGOL DS1054Z). The range of AC electric voltage applied was 0−10 V in peak value, while the frequency f_E ranged between 350 Hz and 1 MHz. The magnetic field energy source consisted of four air-cored copper solenoid coils of 50 mm inner diameter, 51 mm length, and 400 turns, with a current capacity of 3.5A. The frequency f_B of the magnetic field was 50 Hz for all experiments. This setup allowed for the generation of 2D magnetic fields by arranging the four coils orthogonally in the x-y plane. A custom-made MATLAB program was used to control the strength, frequency, and phase angles of the applied magnetic field. Experimental observations were captured in static images and real-time movies using an inverted optical microscope (Olympus IX71) with a black-and-white camera (EPIX SV643M).

Diffraction Patterns. Particle centroids were extracted from optical images using custom-written MATLAB code. The threshold value was chosen to illuminate individual particles better. The noise was decreased by filling appropriate holes in shape-based filtering. The peripherals were eroded for particles in close contact before their centroids were identified. To calculate the associated diffraction patterns, we evaluated the real part of the structure factor

$$S(\mathbf{q}) = \frac{1}{N}\sum_{i=1}^{N}\sum_{j=1}^{N} e^{2\pi \mathbf{q}\cdot(\mathbf{r}_j-\mathbf{r}_i)} \tag{7}$$

where $\mathbf{q}$ is the wavevector, $\mathbf{r}_i$ is the position vector of particle i, and N is the total number of particles. From the diffraction patterns, we can obtain both inter- and intrastripe spacings.

Simulations Methods. For a monolayer of particles, the simulation box (Figure S3) is a 3D slab with a width L and a height σ. For bilayer structures, the slab height is $\sigma + \Delta z$. We chose the center-to-center separation between the top and bottom layers of colloids to be $\Delta z = 0.7\sigma$, which matched an average separation measured between the top and bottom layers of colloids under typical experimental conditions.[19] We note that while the height of our experimental chamber is ∼100 times the particle diameter, we purposely chose the particle concentration so that the final structures were either a monolayer or a bilayer of particles near the bottom substrate for the convenience of characterization. The reason for particle attraction toward the substrate upon application of an external AC electric field remains elusive, although gravitational force and electric image-dipole dipole interactions due to the conducting nature of the substrate could play a role. In our simulations, we do not explicitly include the substrate−particle interactions. However, we effectively account for the observed confinement of particles into a monolayer or bilayer by fixing the z-coordinate of each particle to be in one of two planes normal to the z-direction, as we have done previously.[23] We color particles in the upper plane blue and those in the lower plane red (i.e., closer to the bottom electrode). The numbers of upper- and lower-layer particles in the simulation box are N_U and N_L, respectively, with the total number of particles $N = N_U + N_L$. The projected area fraction of the particles is $\eta_L = N_L\pi\sigma^2/4L^2$, and we define the ratio γ as the number of particles in the upper layer to the number of particles in the lower layer (i.e., $\gamma = N_U/N_L$).

Monte Carlo (MC) simulations for both the monolayer and bilayer of particles were carried out in the canonical (NVT) ensemble using systems of N = 240, 500, or 1000 particles. They yield very similar results. Periodic boundary conditions were imposed in the x- and y-dimensions, and the minimum image convention was implemented for particle interactions.[24] We chose the reduced temperature $T^* = k_BT/\varepsilon_{LJ}$ = 0.35 (where T is the absolute temperature and k_B is Boltzmann's constant) for all simulations. This temperature is low enough for observing ordered structures but high enough to allow for equilibration within reasonable simulation times. Each simulation was conducted for at least 10^5 MC steps, where we estimated that the system had reached equilibrium. For each MC step, N randomly selected particles were sequentially moved in the x- and y-dimensions while their z-coordinate remained fixed. Particle moves were accepted or rejected according to the Metropolis algorithm.[25] The particle displacements in each direction were randomly selected from a uniform distribution ranging from $-d$ to d, with $d_{max} = 0.1\sigma$, which was chosen such that approximately 30% of the moves were accepted.

ASSOCIATED CONTENT

Supporting Information

The Supporting Information is available free of charge at https://pubs.acs.org/doi/10.1021/acsnano.4c11957.

Additional figures about the experimental setup, colloidal structures formed under a magnetic field only, an illustration of the simulation box, and schematics of the EHD flow (PDF)

Formation of colloidal monolayers under electric and magnetic fields and formation of hierarchical structures (MP4)

Control of chain orientation (MP4)

Aligned bundles formed by the tetramers upon the superposition of a one-dimensional magnetic field B_y = 5.1 mT (AVI)

https://doi.org/10.1021/acsnano.4c11957
ACS Nano XXXX, XXX, XXX−XXX

Butterfly-like heptamers formed under the electric field (E_z = 2.8 × 10^4 V/m and f_E = 450 Hz) reconfigure themselves into aligned bundles with the superposition of a one-dimensional magnetic field (AVI)

AUTHOR INFORMATION

Corresponding Authors

David T. Wu − *Department of Chemistry and Department of Chemical and Biological Engineering, Colorado School of Mines, Golden, Colorado 80401, United States; Institute of Chemistry, Academia Sinica, Nangang 115, Taiwan; Department of Chemical Engineering, National Taiwan University, Taipei 10617, Taiwan*; Email: davidwu@sinica.edu.tw

Ning Wu − *Department of Chemical and Biological Engineering, Colorado School of Mines, Golden, Colorado 80401, United States*; orcid.org/0000-0002-2167-3621; Email: ningwu@mines.edu

Authors

Md Ashraful Haque − *Department of Metallurgical and Materials Engineering, Colorado School of Mines, Golden, Colorado 80401, United States*

Joseph R. Maestas − *Department of Chemistry, Colorado School of Mines, Golden, Colorado 80401, United States*

Xingrui Zhu − *Department of Chemical and Biological Engineering, Colorado School of Mines, Golden, Colorado 80401, United States*

Benjamin L. Hanson − *Department of Physics, Colorado School of Mines, Golden, Colorado 80401, United States*

Complete contact information is available at: https://pubs.acs.org/10.1021/acsnano.4c11957

Author Contributions

▽M.A.H. and J.R.M. contributed equally to this work.

Notes

The authors declare no competing financial interest.

ACKNOWLEDGMENTS

This work is supported by the National Science Foundation (CBET-1805073 and CBET-2030480).

REFERENCES

(1) Smay, J. E.; Cesarano, J.; Lewis, J. A. Colloidal Inks for Directed Assembly of 3-D Periodic Structures. *Langmuir* **2002**, *18*, 5429−5437.

(2) Holtz, J. H.; Asher, S. A. Polymerized Colloidal Crystal Hydrogel FIlms as Intelligent Chemical Sensing Materials. *Nature* **1997**, *389*, No. 4.

(3) Zaidouny, L.; Bohlein, T.; Roth, J.; Bechinger, C. Periodic Average Structures of Colloidal Quasicrystals. *Soft Matter* **2014**, *10*, 8705−8710.

(4) Wang, W.; Lv, X.; Moran, J. L.; et al. A Practical Guide to Active Colloids: Choosing Synthetic Model Systems for Soft Matter Physics Research. *Soft Matter* **2020**, *16*, 3846−3868.

(5) Grzelczak, M.; Vermant, J.; Furst, E. M.; Liz-Marzán, L. M. Directed Self-assembly of Nanoparticles. *ACS Nano* **2010**, *4*, 3591−3605.

(6) Ding, T.; Smoukov, S. K.; Baumberg, J. J. Stamping Colloidal Photonic Crystals: A Facile Way towards Complex Pixel Colour Patterns for Sensing and Displays. *Nanoscale* **2015**, *7*, 1857−1863.

(7) Wang, X. Inverse Colloidal Crystal Membranes: Formation, Surface Modification and Applications. Ph.D.Thesis, Colorado State University, 2010.

(8) Nasilowski, M.; Mahler, B.; Lhuillier, E.; Ithurria, S.; Dubertret, B. Two-Dimensional Colloidal Nanocrystals. *Chem. Rev.* **2016**, *116*, 10934−10982.

(9) Martin, J. E.; Solis, K. J. Fully Alternating, Triaxial Electric or Magnetic Fields Offer New Routes to Fluid Vorticity. *Soft Matter* **2015**, *11*, 241−254.

(10) Byrom, J.; Biswal, S. L. Magnetic Field Directed Assembly of Two-Dimensional Fractal Colloidal Aggregates. *Soft Matter* **2013**, *9*, 9167−9173.

(11) Caleap, M.; Drinkwater, B. W. Acoustically Trapped Colloidal Crystals That Are Reconfigurable in Real Time. *Proc. Natl. Acad. Sci. U.S.A.* **2014**, *111*, 6226−6230.

(12) Edwards, T. D.; Yang, Y.; Beltran-Villegas, D. J.; Bevan, M. A. Colloidal Crystal Grain Boundary Formation and Motion. *Sci. Rep.* **2014**, *4*, No. 6132.

(13) Demirörs, A. F.; Courty, D.; Libanori, R.; Studart, A. R. Periodically Microstructured Composite Films Made by Electric- and Magnetic-Directed Colloidal Assembly. *Proc. Natl. Acad. Sci. U.S.A.* **2016**, *113*, 4623−4628.

(14) Yang, T.; Tasci, T. O.; Neeves, K. B.; Wu, N.; Marr, D. W. M. Magnetic Microlassos for Reversible Cargo Capture, Transport, and Release. *Langmuir* **2017**, *33*, 5932−5937.

(15) Marzo, A.; Drinkwater, B. W. Holographic Acoustic Tweezers. *Proc. Natl. Acad. Sci. U.S.A.* **2019**, *116*, 84−89.

(16) Harraq, A. A.; Choudhury, B. D.; Bharti, B. Field-Induced Assembly and Propulsion of Colloids. *Langmuir* **2022**, *38*, 3001−3016.

(17) Demirörs, A. F.; Beltramo, P. J.; Vutukuri, H. R. Colloidal Switches by Electric and Magnetic Fields. *ACS Appl. Mater. Interfaces* **2017**, *9*, 17238−17244.

(18) Ma, F.; Wang, S.; Wu, D. T.; Wu, N. Electric-Field−Induced Assembly and Propulsion of Chiral Colloidal Clusters. *Proc. Natl. Acad. Sci. U.S.A.* **2015**, *112*, 6307−6312.

(19) Ma, F.; Wu, D. T.; Wu, N. Formation of Colloidal Molecules Induced by Alternating-Current Electric Fields. *J. Am. Chem. Soc.* **2013**, *135*, 7839−7842.

(20) Heatley, K. L.; Ma, F.; Wu, N. Colloidal Molecules Assembled from Binary Spheres under an AC Electric Field. *Soft Matter* **2017**, *13*, 436−444.

(21) Yang, Y.; Pham, A. T.; Cruz, D.; Reyes, C.; Wiley, B. J.; Lopez, G. P.; Yellen, B. B. Assembly of Colloidal Molecules, Polymers, and Crystals in Acoustic and Magnetic Fields. *Adv. Mater.* **2015**, *27*, 4725−4731.

(22) Grob, D. T.; Wise, N.; Oduwole, O.; Sheard, S. Magnetic Susceptibility Characterisation of Superparamagnetic Microspheres. *J. Magn. Magn. Mater.* **2018**, *452*, 134−140.

(23) Maestas, J. R.; Ma, F.; Wu, N.; Wu, D. T. Electric-Field-Driven Assembly of Dipolar Spheres Asymmetrically Confined between Two Electrodes. *ACS Nano* **2021**, *15*, 2399−2412.

(24) Allen, M.; Tildesley, D. *Computer Simulations of Liquids*; Oxford University Press: New York, 1987.

(25) Metropolis, N.; Rosenbluth, A. W.; Rosenbluth, M. N.; Teller, A. H.; Teller, E. Equation of State Calculations by Fast Computing Machines. *J. Chem. Phys.* **1953**, *21*, 1087−1092.

(26) Ignaczak, W.; Sui, X.; Kellersztein, I.; Wagner, H. D.; El Fray, M. The Effect of Fibre Sizing and Compatibilizer of Polypropylene/Poly(Butylene Terephthalate) Blends on the Mechanical and Interphase Properties of Basalt Fibre Reinforced Composites: Basalt-Fibre Reinforced Composites. *Polym. Int.* **2018**, *67*, 414−421.

(27) Lin, Z.; Liu, Y.; Raghavan, S.; Moon, K.; Sitaraman, S. K.; Wong, C. Magnetic Alignment of Hexagonal Boron Nitride Platelets in Polymer Matrix: Toward High Performance Anisotropic Polymer Composites for Electronic Encapsulation. *ACS Appl. Mater. Interfaces* **2013**, *5*, 7633−7640.

(28) Fan, X.; Walther, A. 1D Colloidal Chains: Recent Progress from Formation to Emergent Properties and Applications. *Chem. Soc. Rev.* **2022**, *51*, 4023−4078.

(29) Sander, J. S.; Erb, R. M.; Li, L.; Gurijala, A.; Chiang, Y.-M. High-Performance Battery Electrodes via Magnetic Templating. *Nat. Energy* **2016**, *1*, No. 16099.
(30) Li, L.; Erb, R. M.; Wang, J.; Wang, J.; Chiang, Y. M. Fabrication of Low-Tortuosity Ultrahigh-Area-Capacity Battery Electrodes through Magnetic Alignment of Emulsion-Based Slurries. *Adv. Energy Mater.* **2019**, *9*, No. 1802472.
(31) Seo, Y. P.; Han, S.; Choi, J.; Takahara, A.; Choi, H. J.; Seo, Y. Searching for a Stable High-Performance Magnetorheological Suspension. *Adv. Mater.* **2018**, *30*, No. 1704769.
(32) Wen, W.; Huang, X.; Sheng, P. Electrorheological Fluids: Structures and Mechanisms. *Soft Matter* **2008**, *4*, 200−210.
(33) Martin, J. E.; Snezhko, A. Driving self-assembly and emergent dynamics in colloidal suspensions by time-dependent magnetic fields. *Rep. Prog. Phys.* **2013**, *76*, No. 126601.
(34) Squires, T. M.; Bazant, M. Z. Induced-Charge Electro-Osmosis. *J. Fluid Mech.* **1999**, *509*, 217−252.
(35) Ristenpart, W. D.; Aksay, I. A.; Saville, D. Electrohydrodynamic Flow Around a Colloidal Particle Near an Electrode With an Oscillating Potential. *J. Fluid Mech.* **2007**, *575*, 83−109.
(36) Fernández-Mateo, R.; García-Sánchez, P.; Calero, V.; Morgan, H.; Ramos, A. Stationary Electro-Osmotic Flow Driven by AC Fields around Charged Dielectric Spheres. *J. Fluid Mech.* **2021**, *924*, No. R2.
(37) Bharti, B.; Kogler, F.; Hall, C. K.; Klapp, S. H.; Velev, O. D. Multidirectional Colloidal Assembly in Concurrent Electric and Magnetic Fields. *Soft Matter* **2016**, *12*, 7747−7758.
(38) Bharti, B.; Velev, O. D. Assembly of Reconfigurable Colloidal Structures by Multidirectional Field-Induced Interactions. *Langmuir* **2015**, *31*, 7897−7908.
(39) Yethiraj, A. Tunable Colloids: Control of Colloidal Phase Transitions with Tunable Interactions. *Soft Matter* **2007**, *3*, 1099−1115.
(40) Yang, X.; Johnson, S.; Wu, N. The Impact of Stern-Layer Conductivity on the Electrohydrodynamic Flow Around Colloidal Motors under an Alternating Current Electric Field. *Adv. Intell. Syst.* **2019**, *1*, No. 1900096.
(41) Ristenpart, W. D.; Aksay, I. A.; Saville, D. A. Electrohydrodynamic Flow around a Colloidal Particle near an Electrode with an Oscillating Potential. *J. Fluid Mech.* **2007**, *575*, 83−109.

https://doi.org/10.1021/acsnano.4c11957
ACS Nano XXXX, XXX, XXX−XXX